Distinct Structural Changes Detected by X-Ray Fiber Diffraction in Stabilization of F-Actin by Lowering pH and Increasing Ionic Strength

Toshiro Oda,*† Kouji Makino,*† Ichiro Yamashita,* Keiichi Namba,*‡ and Yuichiro Maéda*†

*International Institute for Advanced Research, Matsushita Electric Industrial Co. Ltd., Seika, Kyoto 619-0237, †Laboratory for Structural Biochemistry, RIKEN Harima Institute, Mikazuki, Hyogo 679-5148, and ‡Protonic Nano-Machine Project, ERATO, JST, Seika, Kyoto 619-0237, Japan

ABSTRACT   Lowering pH or raising salt concentration stabilizes the F-actin structure by increasing the free energy change associated with its polymerization. To understand the F-actin stabilization mechanism, we studied the effect of pH, salt concentration, and cation species on the F-actin structure. X-ray fiber diffraction patterns recorded from highly ordered F-actin sols at high density enabled us to detect minute changes of diffraction intensities and to precisely determine the helical parameters. F-actin in a solution containing 30 mM NaCl at pH 8 was taken as the control. F-actin at pH 8, 30 to 90 mM NaCl or 30 mM KCl showed a helical symmetry of 2.161 subunits per turn of the 1-start helix (12.968 subunits/6 turns). Lowering pH from 8 to 6 or replacing NaCl by LiCl altered the helical symmetry to 2.159 subunits per turn (12.952/6). The diffraction intensity associated with the 27-Å meridional layer-line increased as the pH decreased but decreased as the NaCl concentration increased. None of the solvent conditions tested gave rise to significant changes in the pitch of the left-handed 1-start helix (~59.8 Å). The present results indicate that the two factors that stabilize F-actin, relatively low pH and high salt concentration, have distinct effects on the F-actin structure. Possible mechanisms will be discussed to understand how F-actin is stabilized under these conditions.

INTRODUCTION

In living cells, actin is rapidly turned over between the monomeric (G-actin) and polymeric (F-actin) forms. The reversible G-F transition is modulated by binding of actin-binding proteins, either by stabilizing or depolymerizing F-actin or sequestering G-actin. F-actin is organized to form higher-order structural networks. The actin network is continuously reorganized in response to external signals. For viability of the cell, the dynamic property of the actin cytoskeleton is essential (Belmont and Drubin, 1998). To understand the mechanism underlining the dynamic property of the network, detailed knowledge is required on the mechanism of actin polymerization and how it is regulated by actin-binding proteins.

The pioneering thermodynamic and kinetic studies by Oosawa and his colleagues (Oosawa and Kasai, 1971; also reviewed by Korn, 1982; Carlier, 1991) have elucidated that actin polymerization is a condensation phenomenon and is regulated by hydrolysis of bound ATP. G-actin polymerizes in vitro upon addition of salt if the G-actin concentration is higher than the critical concentration. Once equilibrium is reached between F-actin and G-actin, the concentration of G-actin remains at the critical concentration. The critical concentration (C_c) is related to the interaction free energy ($-\epsilon$) of G-actin monomers added to the end of a filament through the relation of $\ln C_c = -\epsilon/k_B T$, where k_B is the Boltzmann constant. The lower the critical concentration, the more stable is the F-actin structure. The critical concentration decreases, and thereby F-actin is stabilized as the solvent pH decreases or the ionic strength increases or when LiCl is used as the polymerizing salt (Pan and Ware, 1988; Zimmerle and Frieden, 1988b; Wang et al., 1989; Colombo et al., 1991). In the present study, we have addressed the question whether or not the structures of F-actin are the same under all these F-actin stabilizing conditions.

Because the crystal structure of DNase I-actin complex was obtained in 1990 (Kabsch et al., 1990), structural changes associated with the function of F-actin, such as actin polymerization and interactions with actin-binding proteins, have been searched for. Electron microscopic studies have been interpreted to indicate that the conformation of actin is variable and dependent on bound nucleotides, bound cations, and the association of actin-binding proteins (Bremer et al., 1991; Orlova and Egelman, 1992, 1993, 1995; Orlova et al., 1995; Lepault et al., 1994; McGough et al., 1997).

In the present study, structural information has been collected from x-ray fiber diffraction patterns recorded from liquid-crystalline sols of F-actin oriented in quartz capillaries under various solvent conditions. The advantage of using sols is that a high degree of orientation and high protein concentration allow highly sensitive detection of structural changes, including changes in the helical symmetry of F-actin. The present results indicate that there are at least two types of distinct structural changes that stabilize F-actin; the structural changes caused by lowering the pH are distinct from those caused by increasing the ionic strength.

MATERIALS AND METHODS

X-ray diffraction and data processing

Actin was prepared from acetone powder of rabbit skeletal muscle according to the method of Spudich and Watt (1971) with minor modifications, followed by one step further purification by chromatography on Sephadex G-150. Gelsolin was prepared from bovine serum according to the method of Kurokawa et al., (1990).

Actin was polymerized by adding KCl (the final concentration of 60 mM) to a mixture of G-actin and gelsolin (with a typical molar ratio, 100:1) in G-buffer containing 1 mM $NaHCO_3$, 0.1 mM $CaCl_2$, 0.2 mM ATP, 1 mM NaN_3, and 1 mM 2-mercaptoethanol, followed by solvent exchange by dialysis for 1–2 days against various solutions. F-actin sols were prepared in quartz capillaries as described previously (Oda et al., 1998). The standard solvent condition used in the present study was 30 mM NaCl, 10 mM Tris-acetate (pH 8), 1 mM $CaCl_2$, 0.5 mM ATP, 1 mM 2-mercapto-ethanol, and 1 mM NaN_3. For various solvent conditions, the salt used was either NaCl, LiCl, or KCl at concentrations of 30, 60, or 90 mM, and the pH was altered by replacing the pH buffer either with Tris-acetate (pH 7.5, 8, or 8.5) or BisTris-acetate (pH 6, 6.5, or 7). X-ray fiber diffraction patterns were recorded on imaging plates (IPs, 20 cm × 25 cm) using an RU-200 x-ray generator with a double-mirror optics (Rigaku, Osaka, Japan). Average exposure time was 10 h and the specimen-to-film distance was ~166 mm. The accurate specimen-to-film distance was determined from the powder pattern of $CaSO_4 \cdot 2H_2O$ crystals ($a_0 = 6.2846$ Å, $b_0 = 15.2011$ Å, $c_0 = 5.6737$ Å, $\beta = 114.10°$) placed at the same position as F-actin sols; reflections (020), (021), and (040) were used as standards (Yamashita et al., 1998). Imaging plates were scanned at a raster size of 0.1 mm using a BA100 IP reader (Fuji Film, Odawara, Japan). The diffraction patterns were processed so that the four quadrants were averaged, circular-symmetric background was subtracted, and the intensities were mapped into the reciprocal space. The processed diffraction patterns were expressed in the polar coordinates with a radial step dependent on the resolution such as ~0.00039 Å^{-1} at low resolution and an angular step of 0.5° (the equator: 0°).

Well-oriented F-actin sols are necessary for collection of diffraction patterns of F-actin with a good quality. In the previous studies, we found that control of filament length by a capping protein gelsolin was effective for improvement of the filament orientation in sols (Oda et. al., 1998). We used gelsolin to record the diffraction patterns. The binding of gelsolin is reported to modify the structure of F-actin (Orlova et al., 1995; Suzuki and Ito, 1996; Prochniewicz et al., 1996; Khaitlina and Hinssen, 1997). Although their finding is interesting, we cannot refer to this point from present results.

Determination of the helical parameters of F-actin from diffraction patterns

F-actin is a filament of a helical symmetry (Oosawa and Kasai, 1962; Hanson and Lowy, 1963). The helical arrangement of asymmetric units is characterized by a set of three parameters, (u, t, and P) or (u, t, and p) (Cochran et al., 1952; Klug et al., 1958); u asymmetric units are distributed evenly in t turns of the basic helix within the axial repeat P. The pitch of the basic helix is given by $p = P/t$ and the helical symmetry is defined as u/t. In the case of F-actin, the asymmetric unit consists of one actin molecule, the basic helix is the 1-start left-handed helix with a pitch of ~59 Å, and the helical symmetry of F-actin approximates to 13/6 (Hanson and Lowy, 1963; Huxley and Brown, 1967). Based on theses parameters, the helical symmetry and helical pitch of F-actin were refined based on the diffraction image data as previously described (Oda et al., 2000). In short, three parameters were obtained from each diffraction pattern: the pitch of the 1-start left-handed helix (p), the helical symmetry (u/t) and the angular distribution of the filament orientation (α). In this analysis, we used two-dimensional profile fitting program (Yamashita et al., 1995, 1998;

Hasegawa, Yamashita, and Namba, in preparation). The software sets point-spread functions for given α and the beam size along each layer-line at an interval of 0.001 Å^{-1}, of which positions are determined for given p and u/t. The height of each point-spread function was adjusted to fit the observed diffraction pattern. Finally, the intensity residuals between the generated and observed patterns were calculated. By monitoring the residuals in selected regions on the diffraction pattern while manually giving p, α, and u/t one by one, the three parameters were optimized one after the other. First, the axial position of the 59-Å layer-line, i.e., the pitch of the left-handed 1-start helix p, was determined from the minimum of the residual obtained around the 59-Å layer-line with fixed α and u/t. Secondly, α was optimized using the intensity distribution around the 59-Å layer-line with the fixed p and u/t. Finally, u/t was determined from the axial positions of the 51-Å and 59-Å layer-lines with fixed α and p. In this way, one set of α, p, and u/t was self-consistently determined from a single diffraction pattern. The helical symmetry u/t may also be expressed as the number of subunits per 6 turns so as to be compared with a well-known symmetry of 13/6.

In Fig. 1, a and b, residual plots for a typical diffraction pattern are shown to demonstrate the accuracy of the method used to determine the structural parameters p and u/t. The curves of residuals are smooth, indicating that these parameters can be determined at least at the accuracy of the interval of the residual calculation used here. Fig. 1 b also indicates that the accuracy in the determination of u/t is hardly affected by the slight ambiguity in p. To see the effect of noise level in intensity on the accuracy of the parameter determination, we carried out simulation experiments of the parameter determination using diffraction patterns calculated from a set of experimentally measured layer-line intensities with artificial noises calculated by the Monte-Carlo method (Press et al., 1994). A set of diffraction patterns was generated by adding artificial noises whose amplitudes have the following statistics. The noises were assumed to have a Gaussian distribution with a standard deviation of a multiple of the square root of the intensities. The multiplication factor was determined so that the residuals for the p determination were at the same level as those obtained from experimental data. From these simulated patterns, the pitches were determined by the same procedure at the finer interval, which is 0.0016 Å. The results are summarized in Fig. 1 c. The values of p obtained from the simulated patterns are predominantly within a range of ±0.01 Å around the mean, and this is the estimated error of the pitch determination from individual diffraction patterns. In the actual data processing for the p determinations, the errors were estimated at the interval of ±0.016 Å.

Layer-line intensities (I) were obtained, in the region up to 0.05 Å^{-1} (20-Å resolution) with a radial step of 0.001 Å^{-1}, using the two-dimensional profile fitting program. For this procedure the helical symmetry was assumed to be either 67/31 or 136/63 and the Bessel terms up to the sixth order were included.

Quantitative comparison of overall layer-line intensity profiles and the intensity of the 27-Å layer-line

For quantitative comparison of the overall layer-line intensity profiles between diffraction patterns, R-factor was calculated as

$$R(\%) = \frac{\sum |I_{ph8}^{1/2} - k \times I^{1/2}|}{\sum I_{ph8}^{1/2}} \times 100.$$

Here, k is the scaling factor and I is the extracted layer-line intensity. The square root of intensity, $I^{1/2}$, represents the amplitudes obtained from F-actin under various solvent conditions, and the amplitude $I_{ph8}^{1/2}$ represents those obtained from F-actin in the standard condition of pH 8 and 30 mM NaCl, for which multiple diffraction patterns were processed and averaged. The R-factors were calculated within a resolution range from 0.012 to 0.042 Å^{-1}.
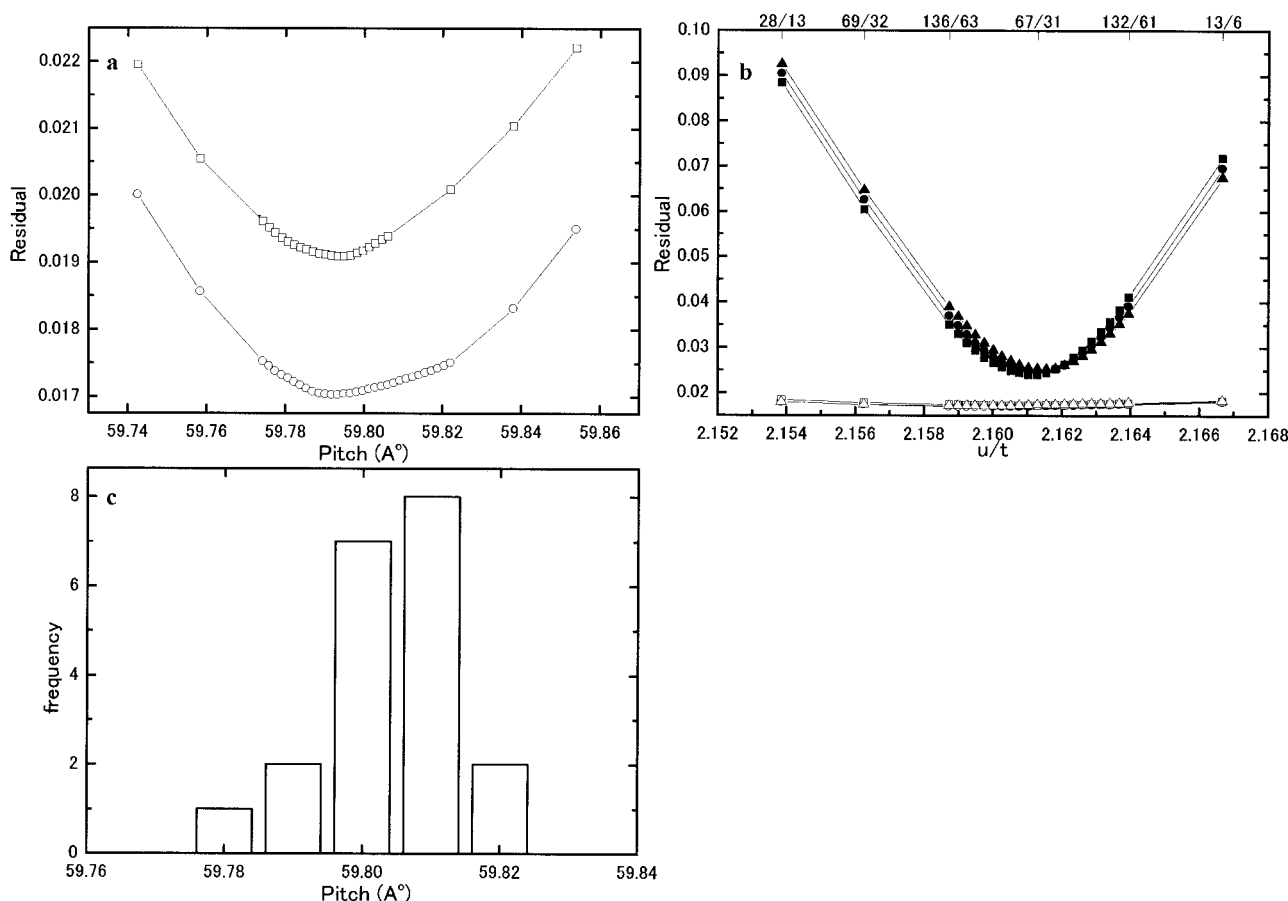
FIGURE 1 Demonstration of the accuracy of the method used to determine the structural parameters. Typical residual plots used for the determination of the pitch p of the left-handed 1-start helix and the helical symmetry u/t of F-actin are shown in a and b, respectively. In a, the residuals were calculated around the 59-Å layer-line (in the region of radius $0.0179–0.0191$ Å^{-1} and the angle θ of 55–70°) with a step of either ~0.016 Å^{-1} (coarse) or ~0.0016 Å^{-1} (fine). With $\alpha = 3.1$ (an unoptimized value; $\square$) and $\alpha = 3.22$ (the optimized value; $\bigcirc$), the pitch $p = 59.795$ Å and $p = 59.792$ Å were obtained, respectively, indicating that the determined pitch is hardly affected by the noise in the diffraction intensities and the ambiguity of α. In b, the residuals were calculated in the region around the 59-Å layer-line (*open symbols*) or around the 51-Å layer-line (in the area of radius of $0.0195–0.0215$ Å^{-1} and the angle θ of 65–70°; *closed symbols*) for fixed p at relatively large intervals of u/t, such as 28/13 (indicated above the frame of the graph; 2.154), 69/32 (2.156), 136/63 (2.159), 67/31 (2.161), 132/61 (2.164), and 13/6 (2.167), as well as at finer intervals ($\sim1/10$) between 136/63 (2.159) and 132/61 (2.164) such as 771/1322, 178/332, etc. The residual plot is also smooth. The symmetry u/t was determined with three different values of pitch p, 59.775 ($\blacksquare$), 58.792 (the optimal value; $\bullet$), 58.808 Å ($\blacktriangle$) as 67/31(2.1613), 67/31(2.1613), and 719/1338(2.1616), respectively, indicating that the ambiguity of pitch p hardly affects the determination of u/t. In the actual parameter determination carried out in this study, the best-fit symmetry was determined by interpolating the residuals obtained at relatively large intervals by use of a spline function. This procedure was rationalized by confirming that the best-fit symmetry obtained using the residuals calculated at finer u/t was not significantly different from that obtained using the interpolation procedure. (*c*) Distribution of pitches determined from 20 simulated diffraction patterns with noises at a certain level. The mean and the standard deviation of the histogram were 59.804 Å and 0.0096 Å, respectively, whereas the pitch obtained from the noise-free simulated pattern was 59.801 Å. To make the residuals at the same level (0.0161) as that of a, the standard deviation of the noise artificially put into the simulated patterns was set to be 5.29 times the square root of the intensity of the pattern.

To compare the intensities associated with the meridional 27-Å layer-line of different patterns, its amplitude sum within a radial range of $0.001–0.008$ Å^{-1} were normalized against the amplitude sum on the 59-Å layer-line within a radial range of $0.001–0.048$ Å^{-1} as

$$I_{relative}^{1/2} = \frac{\sum_{0.001}^{0.008} I_{27layer-line}^{1/2}}{\sum_{0.001}^{0.0048} I_{59layer-line}^{1/2}}.$$

Measurement of fluorescence increment of pyrenyl-actin and the critical concentration

Pyrenyl-actin was prepared according to the method of Kouyama and Mihashi (1981). The experiments to measure the fluorescence intensity were performed using F-actin preparations consisting of 95% unmodified actin and 5% pyrenyl-actin. Actin was polymerized at a series of actin concentrations (1–7 μM) in various solvents. The standard solvent condition was 30 mM NaCl, 10 mM Tris-acetate (pH 8), 1 mM CaCl$_2$, 0.5 mM ATP, 0.25 mM NaN$_3$, 0.25 mM NaHCO$_3$, and 0.25 mM 2-mercaptoethanol. For higher salt concentrations, NaCl was added to final concentrations from 30 to 100 mM, whereas, for lower pH, the pH buffer was replaced by 10 mM Tris-acetate for pH 7.5 and by 10 mM BisTris-acetate for pH 7, 6.5, or 6. After incubation in one of these solvents at 20°C for 1 day, the fluorescence of pyrenyl-actin was measured using a Hitachi fluorescence spectrometer F3100 with the excitation wavelength at 365 nm and the emission at 407 nm. The concentration of labeled actin was measured using Protein assay kit (Pierce Chemical Co., Tokyo, Japan).

RESULTS

Environment of the C-terminal region, pyrene-Cys-374, in the F-actin state

We first confirmed the effect of the ionic strength and the solvent pH on the stability of F-actin under solvent conditions close to those used for our diffraction experiments. Low salt concentrations were used to collect diffraction patterns of high quality because they are favorable for good orientation of F-actin sols. We measured the critical concentration of actin polymerization using samples containing 5% pyrenyl-actin, which increases the fluorescence intensity by approximately 20-fold upon polymerization (Kouyama and Mihashi, 1981). Data from fluorescence measurements for monitoring actin polymerization as a function of the actin concentration are shown in Fig. 2. Data in Fig. 2, *a* and *b*, are representative for different pH values and salt concentrations, respectively, and Fig. 2, *c* and *d*, show the summaries of such data. The critical concentration

decreased by lowering the solvent pH from 8 to 6 as in Fig. 2 *c*, and it decreased with increase in the salt concentration from 30 mM to 60 mM as in Fig. 2 *d*. The critical concentration reached a constant value of ~1.3 μM actin at NaCl concentrations higher than 60 mM. These results confirmed that decrease in the solvent pH and increase in the salt concentration both stabilize F-actin.

Conformational differences of F-actin under various solvent conditions can be detected as the fluorescence intensity from pyrene that labels Cys-374 near the C-terminus of actin. It is believed that the environment of pyrene is altered by incorporation of G-actin into F-actin and/or by structural change associated with it. The fluorescence intensity change is dependent on the conformation of Cys-374 in the C-terminal region, which has been postulated to switch between a couple of different conformations under various conditions (Orlova and Egelman, 1995). Moreover, it is known that the increment in the fluorescence intensity is dependent on bound nucleotides and with or without cleav-
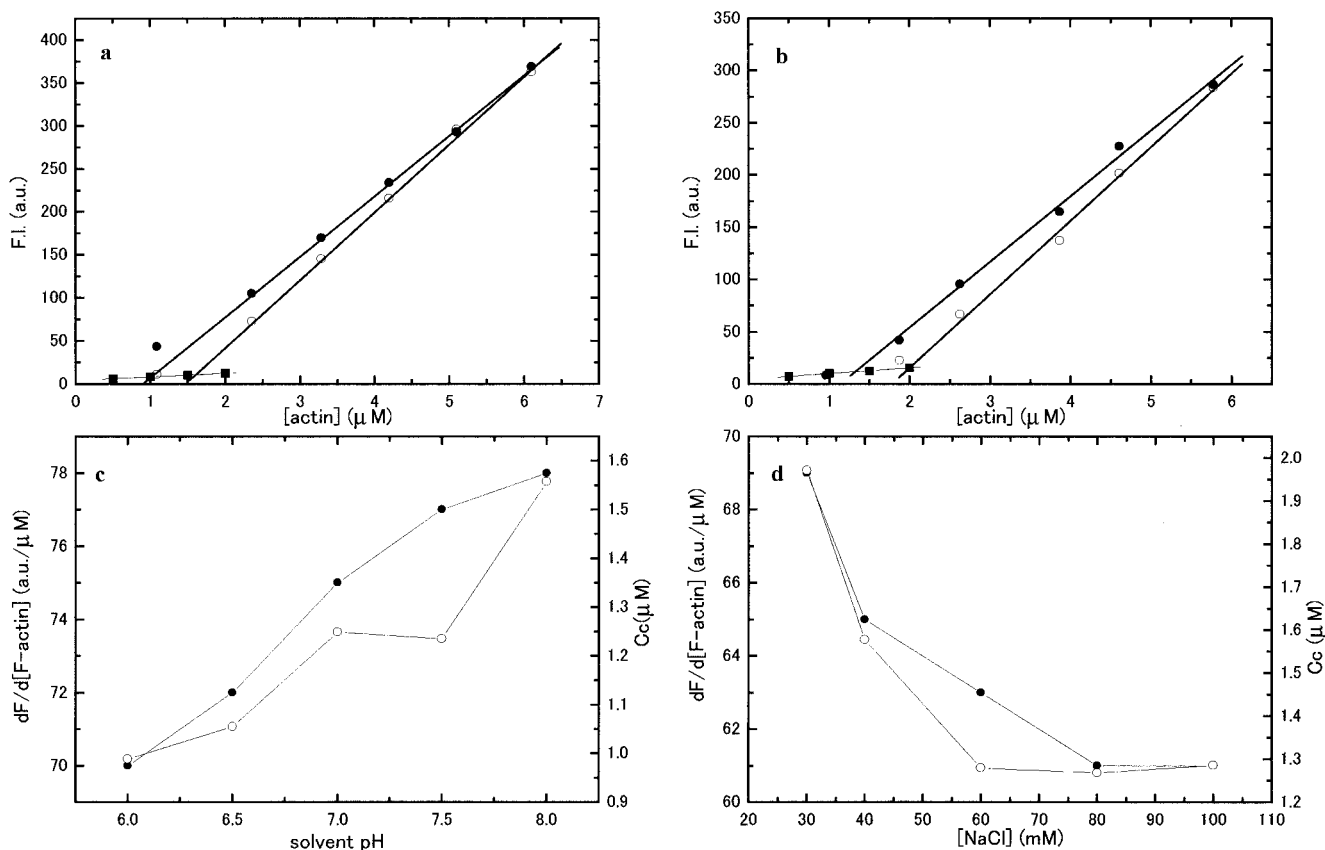

FIGURE 2   Influence of the solvent pH and salt concentration to the stability of F-actin. (*a*) The fluorescence intensity of pyrenyl actin versus the concentration of total actin at pH 6 (●) or at pH 8 (○). The fluorescence intensity was measured after actin polymerization for 1 day at 20°C, in solutions containing 30 mM NaCl, 10 mM Tris-acetate (pH 6) or BisTris-acetate (pH 8), 1 mM $CaCl_2$, 0.5 mM ATP, 0.5 mM, $NaHCO_3$, 0.25 mM NaN_3, and 0.25 mM 2-mercaptoethanol. ■, actin in the G-buffer. (*b*) The fluorescence intensity of pyrenyl actin versus total actin in the presence of 100 mM NaCl (●), 30 mM NaCl (○), or in the G-buffer (■). The solution conditions were the same as in *a* except that the measurements were carried out at pH 8. (*c* and *d*) The slope (●) and the critical concentration (○) obtained from the graphs, like *a* and *b* are plotted against the solvent pH (*c*) or against the NaCl concentration (*d*). The slope dF/d[F-actin] was calculated using a linear regression for the liner portion (2.4–6.2 μM actin in *a* and 1.9–5.8 μM actin in *b*).

age of subdomian 2 of actin (A. Ooi and K. Mihashi, personal communication; Khaitlina et al., 1993), each of which may be associated with an overall conformational change of F-actin. Therefore, the increment in the fluorescence intensity per increment in the amount of F-actin, dF/d[F-actin], is dependent on the F-actin conformation. As shown in Fig. 2, *a* and *b*, the slope (dF/d[F-actin]) decreases as pH decreases or the NaCl concentration increases, and these behaviors are closely associated with the change of the critical concentration C_c, as is more clearly shown in Fig. 2 *c* (at various solvent pH values) and Fig. 2 *d* (at various salt concentrations). This indicates that some conformational changes of actin associated with the fluorescence increase from pyrene at Cys-374 is concomitant with the filament stabilization, regardless of whether it is caused by lowering the pH or by increasing the salt concentration, although this interpretation leaves an ambiguity because the pyrene labeling at Cys-374 itself may change the structure of F-actin.

Helical structure of F-actin

To directly study the structural differences of F-actin, x-ray diffraction patterns were collected from well-oriented F-actin sols in various solvent conditions. Helical parameters of F-actin were precisely determined and used as an indicator representing the overall filament structure.

First, we determined the axial position of the 59-Å layer-line p with high precision using a profile fitting procedure (Yamashita et al., 1995, 1998; Oda et al., 1998, 2000). As shown in Fig. 3, the pitch was determined to be 59.8(2) $\pm$ 0.06 Å (mean $\pm$ SD) in the standard solvent containing 30 mM NaCl, 10 mM Tris-acetate (pH 8.0) (the control F-actin

structure). From 10 samples at pH 6, the pitch was estimated to be 59.7(5) $\pm$ 0.05 Å. From six samples in 30 mM LiCl in replacement of 30 mM NaCl, the pitch was 59.7(7) $\pm$ 0.05 Å. The average pitch from seven samples in the presence of 30 mM KCl was 59.8(0) $\pm$ 0.03 Å. Furthermore, the pitch was not dependent on the salt concentration for 30, 60, and 90 mM NaCl. In conclusion, the pitch p of the left-handed 1-start helix is not dependent significantly on solvent conditions, such as pH, salt concentration, and species of cations.

With the fixed axial position of the 59-Å layer-line as determined above, we carried out two-dimensional profile fitting of the observed diffraction pattern to find the best-fit helical symmetry from the following u/t: 13/6, 132/61, 67/31, 136/63, 69/32, or 28/13. The smallest intensity residual obtained in a region around the 51-Å layer-line was used to find the best fit. The symmetry of u/t = 2.161 (SD = 0.001, n = 38) gave the smallest residual in most cases for the standard solvent condition, 30 mM NaCl at pH 8. This symmetry corresponds to 67/31 or 12.968/6. The symmetry remained unchanged for the NaCl concentration increased to 60 or 90 mM, and in the presence of 30 mM KCl in place of NaCl (Fig. 4). On the other hand, at pH 6 or in 30 mM LiCl in place of NaCl, a symmetry u/t = 2.159 was obtained. The standard deviation was 0.00051 (n = 10) for pH 6, whereas it was 0.00066 (n = 6) for LiCl. This symmetry corresponds to 136/63 or 12.952/6. The change of the helical symmetry from 2.161 to 2.159 is small but statistically significant. With the t-test, the l-value between at pH 8 and pH 6 is $1.84E$-06, whereas the p-value between at pH8 with NaCl and pH 8 with LiCl is $1.69E$-05. The change corresponds to a slight winding of the left-handed 1-start helix. In other words, the long-pitch,
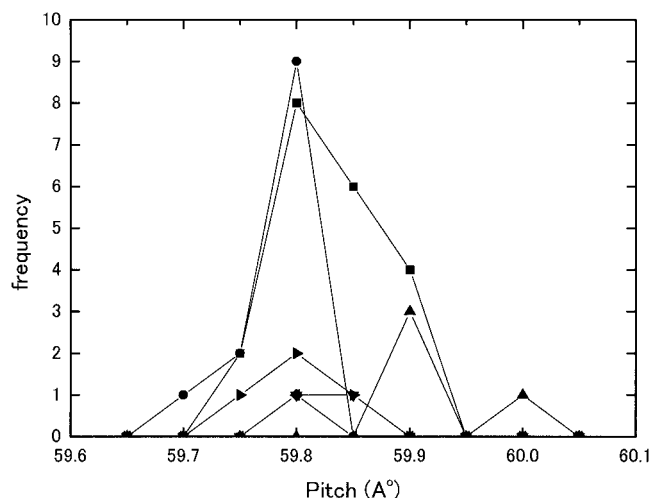

FIGURE 3 Histogram of the pitch of the left-handed 1-start helix of F-actin under the standard condition of 10 mM Tris-acetate (pH 8), 1 mM CaCl$_2$, 0.5 mM ATP, 30 mM NaCl, 1 mM NaN$_3$, and 1 mM 2-mercapto-ethanol. Seven symbols represent data obtained from independent preparations and with slightly different alignments of the camera.
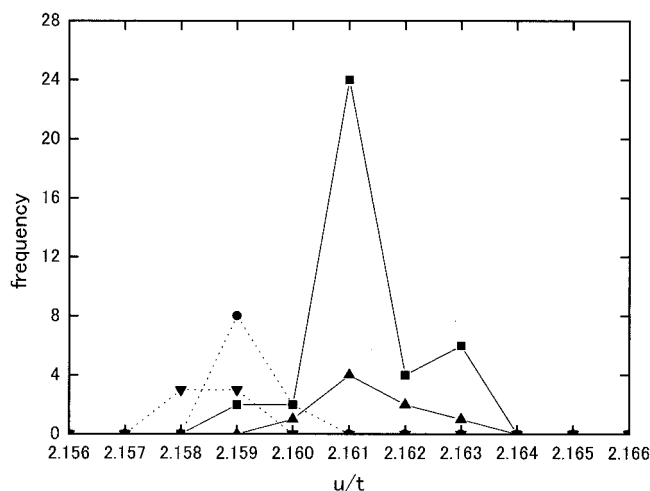

FIGURE 4 Histograms of the helical symmetry of F-actin in the standard condition at pH 8 (■) in the presence of 30 mM NaCl at pH 6 (●) in the presence of 30 mM LiCl (▼) in the presence of 30 mM KCl (▲). The frequency was counted by drop fractions. The helical symmetry was determined as described in the text.

right-handed 2-start actin helix, which has a crossover repeat of ~360 Å, is less twisted. A change of the symmetry in the same direction has been reported by an electron microscopic study upon replacing NaCl by LiCl (Orlova and Egelman, 1992).

Layer-line intensities in various solvent conditions

Fiber diffraction patterns of F-actin are shown in Figs. 5 and 6. The specimens used for these experiments had a similar degree of filament orientation, whose standard angular deviation was 3.2° for the standard condition in 30 mM NaCl at pH 8 (Figs. 5 *a* and 6 *a*), 3.0° for 60 mM NaCl (Fig. 5 *b*), 3.3° for 30 mM KCl (Fig. 5 *c*), 3.6° for 30 mM LiCl (Fig. 5 *d*), and 3.0° in 30 mM NaCl at pH 6 (Fig. 6 *b*). Our previous studies showed that the *R*-factor between two diffraction patterns is dependent on the filament orientation and that diffraction patterns could be compared quantitatively only when the difference in the disorientation angle is within ±0.3° (Oda et al., 2000). Of many diffraction patterns from F-actin collected in the standard condition (30 mM NaCl at pH 8), only those having the filament disorientation angle between 3° and 3.5° were selected. The layer-line amplitude profiles were averaged for six such selected patterns and used as the standard profile. Then, the *R*-factors against the standard profile were calculated for diffraction patterns collected under various solvent conditions. As shown in Table 1, all these *R*-factors were smaller than 10%, showing that the overall profiles of these diffraction patterns are not significantly different from each other. Despite the overall similarity, a close inspection of Figs. 5 and 6 revealed significant differences; the intensity along the 27-Å layer-line in the pattern from F-actin at pH 6 is stronger than that observed at pH 8 (white arrow in Fig. 6). These two amplitude profiles are plotted in Fig. 7. Because this is a meridional layer-line, having the intensity on and near the meridian, the intensity is not very sensitive to the filament disorientation in the sols. For quantitative comparison, the amplitude at the meridian normalized against the
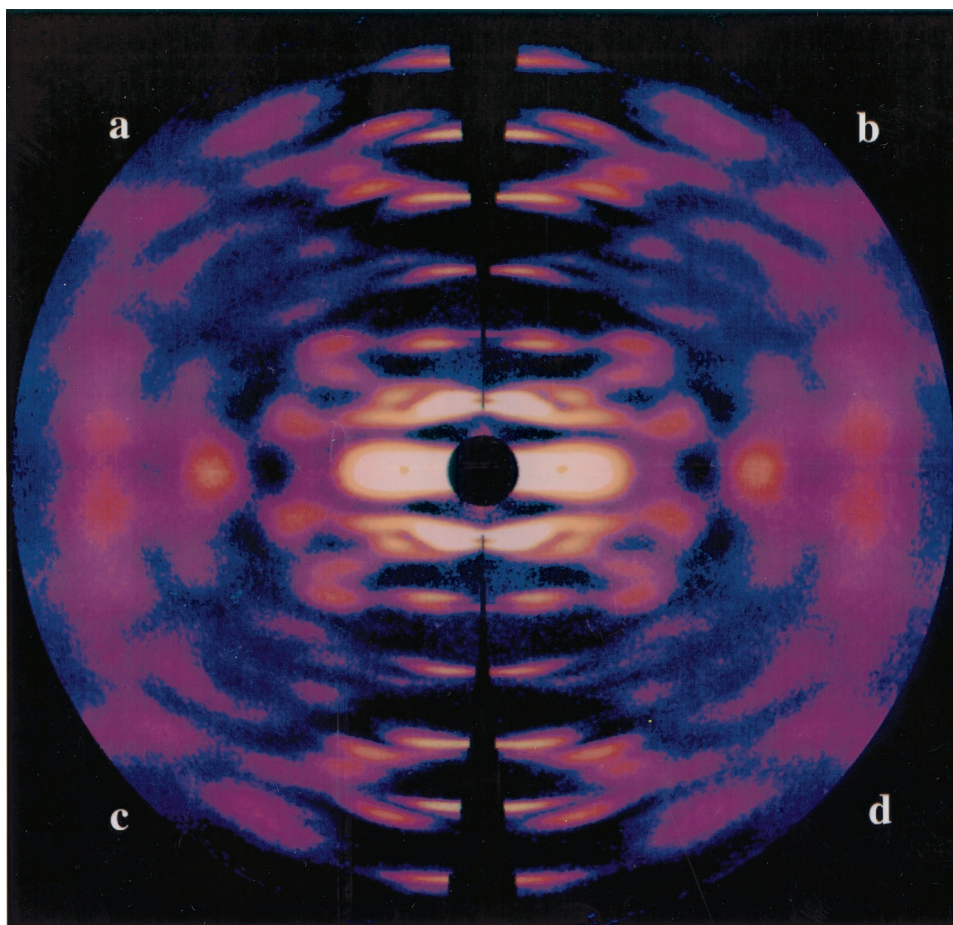

FIGURE 5 Fiber diffraction patterns from F-actin under different solution conditions. Each quadrant corresponds to F-actin in the standard condition of pH 8 in the presence of 30 mM NaCl (*a*), in the presence of 60 mM NaCl (*b*), in the presence of 30 mM KCl (*c*), and in the presence of 30 mM LiCl (*d*). The standard deviation of the angular distribution of the filaments was 3.2° (*a*), 3.0° (*b*) 3.3° (*c*), and 3.6° (*d*). The inner and the outer edge of the pattern correspond to 0.01 Å^{-1} and 0.125 Å^{-1}, respectively.
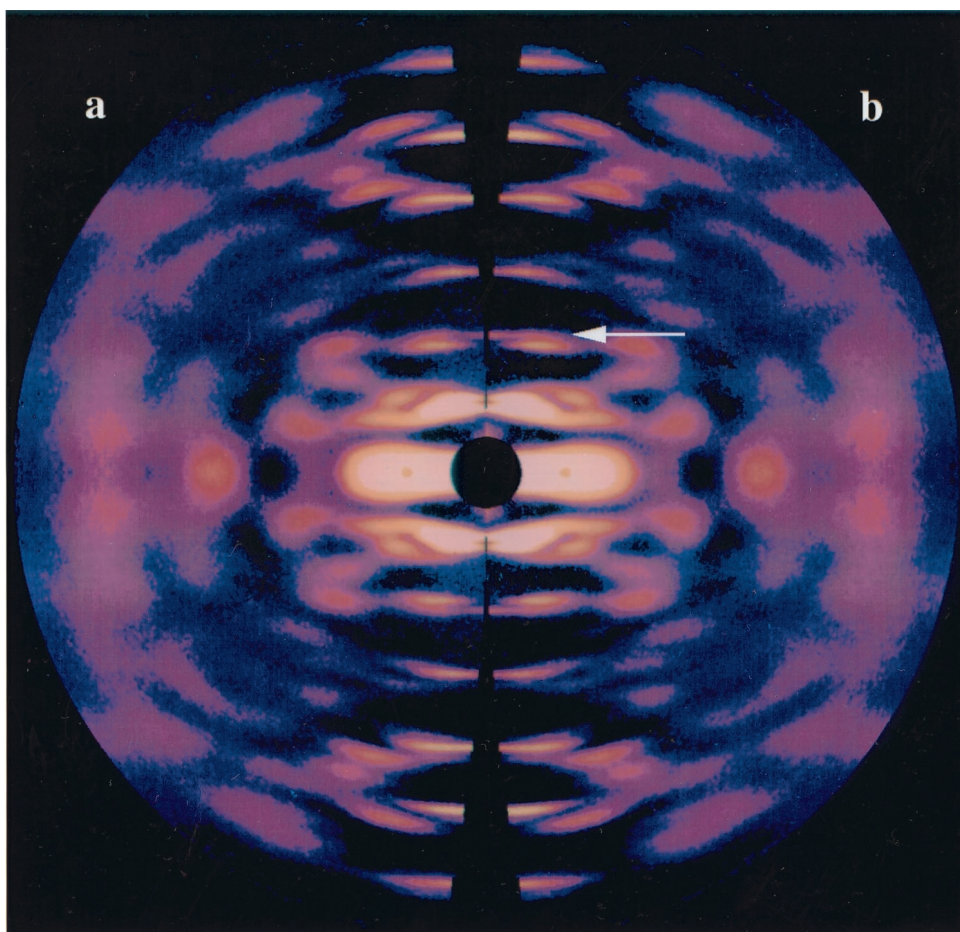
FIGURE 6   Fiber diffraction patterns from F-actin under two different solution conditions. (*a*) F-actin in the standard solution at pH 8 in the presence of 30mM NaCl; (*b*) At pH 6. The standard deviation of the angular distribution of the filaments was 3.2° (*a*) and 3.0° (*b*). The white arrow indicates the 27-Å layer-line. The inner and the outer edge of the pattern correspond to 0.01 Å^{-1} and 0.125 Å^{-1}, respectively.

amplitude of the 59-Å layer-line was calculated, and the results are 0.061 ± 0.003 (*n* = 6) in the standard condition and 0.073 ± 0.002 (*n* = 6) at pH 6. The pH and NaCl concentration dependence of the normalized amplitude are

TABLE 1   *R*-factors of the diffraction patterns of F-actin collected in the various solvent conditions against that in the standard solvent condition

Condition	*R*-factor (%)	Number*
30 mM NaCl at pH 8	–	6
30 mM NaCl at pH 6	3.7	6
30 mM LiCl at pH 8	3.6	2
30 mM KCl at pH 8	4.1	4
60 mM NaCl at pH 8	5.6	1

Of many diffraction patterns from F-actin collected in the standard condition (30 mM NaCl at pH 8), only those having the filament disorientation angle between 3° and 3.5° were selected. For six patterns selected, layer-line amplitude profiles were averaged and used as the standard profile. Against the averaged standard profile, the *R*-factor of each pattern showed a mean value of 2.6 ± 0.6%.

*Number of amplitude profiles that we averaged.

plotted in Fig. 8. As clearly shown in the figure, the meridional amplitude decreased as the solvent pH increased. On the other hands, the meridional amplitude decreased as the NaCl concentration increased from 30 to 90 mM at pH 8. Although the decrease in pH and the increase in the NaCl concentration (at pH 8) both stabilize the F-actin structure as shown in Fig. 2, the former is associated with an increase in the meridional amplitude whereas the latter is associated with a decrease. The results therefore indicate that the structural change induced by lowering pH is distinct from the salt-induced changes.

F-actin in 30 mM LiCl at pH 8 had a normalized meridional amplitude of 0.058 ± 0.002 (*n* = 6). For F-actin in 30 mM KCl at pH 8, the amplitude was 0.060 ± 0.002 (*n* = 7). These are not significantly different from the value obtained in the standard condition (30 mM NaCl at pH 8) but different from that obtained at pH 6. If the F-actin structure is classified in terms of the meridional amplitude of the 27-Å layer-line, F-actin at pH 6 forms one group and that at pH 8 falls into the other group regardless of the cation species.
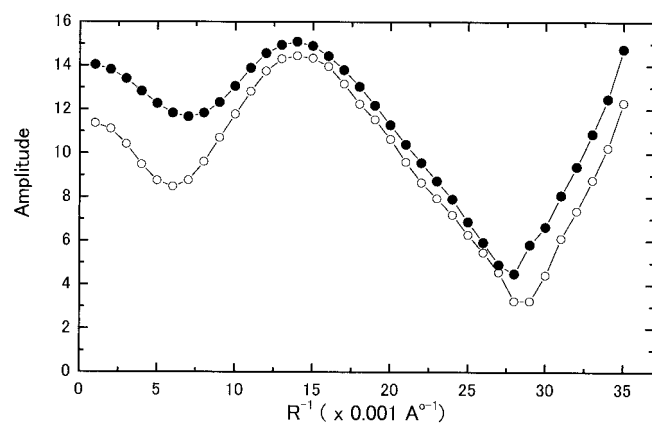
FIGURE 7 Amplitude profile along the 27-Å layer-line at pH 6 (●) and at pH 8 (○). Each profile was obtained by averaging the data from six patterns. The amplitude profiles are plotted at an interval of 0.001 Å^{-1}. The radial position of 0 Å^{-1} corresponds to the meridian.

DISCUSSION

The critical concentration for actin polymerization is reduced, namely, the F-actin state is stabilized, by any of the following changes in the solvent condition: lowering the solvent pH, using LiCl as the polymerizing salt, and increasing the salt concentration (Pan and Ware, 1988; Zimmerle and Frieden, 1988b; Wang et al., 1989; Colombo et al., 1991). We wanted to know whether some common conformational changes in F-actin are associated with the filament stabilization mechanism. Quantitative analysis of x-ray fiber diffraction patterns recorded from well-oriented F-actin sols under various solvent conditions revealed the presence of two types of structural changes. One is the change of the helical symmetry. At pH 8, from 30 to 90 mM NaCl or 30 mM KCl, F-actin has a symmetry of 2.161 subunits per turn of the 1-start helix (12.968/6), whereas the symmetry changes to 2.159 subunits per turn (12.952/6) by decreasing pH to 6 or in the presence of 30 mM LiCl in place of NaCl. The change of the symmetry corresponds to a subtle change in the inter-subunit interactions. The other is an increase in the meridional amplitude of the 27-Å layer-line by decrease in the solvent pH. Because 27 Å is the axial repeat of subunits in F-actin, this meridional amplitude represents the subunit mass distribution projected onto the filament axis. Therefore, the amplitude increase is indicative of a subunit mass rearrangement resulting in more prominent contrast in the 27-Å repeat. These two sorts of conformational changes are independent from each other, as F-actin in 30 mM LiCl at pH 8 showed the change of the first type without the change of the second type. It is also worth noting that the amplitude profile along the 27-Å layer-line was different from that of Holmes' model, most notably the meridional amplitude being ~3-fold stronger, although the other profiles were not significantly different.

From observations of negatively stained F-actin filaments by electron microscopy, Egelman and his colleagues argued
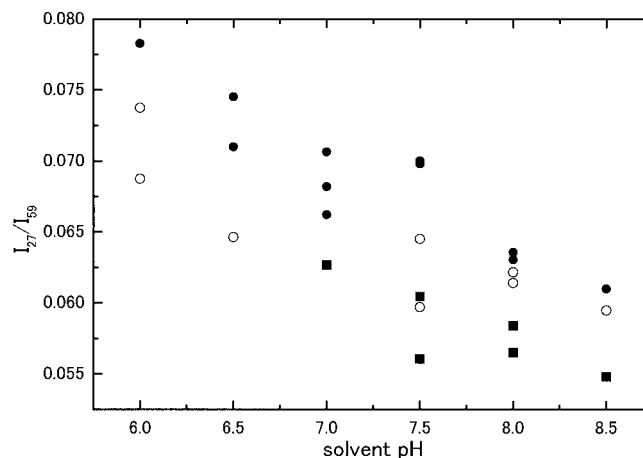

FIGURE 8 Amplitude ratio of the 27-Å layer-line (line in the lateral range from 0.001 to 0.008 Å^{-1}) to the 59-Å layer-line (line in the lateral range from 0.001 to 0.048 Å^{-1}) is plotted against the solvent pH in the presence of different concentrations of salt. ●, 30 mM NaCl; ○, 60 mM NaCl; ■, 90 mM NaCl.

that F-actin is in different conformations depending on the solvent condition (Orlova and Egelman, 1992, 1995; Orlova et al., 1995). Because our systematic investigations on the effects of pH and salt on the F-actin structure were carried out in solution, the results clarify some more details of the structural changes without having to worry about artifacts by staining and drying. Although our present results indicated that replacement of KCl (or NaCl) by LiCl caused a change of the helical symmetry in the same direction as those observed by electron microscopy (Orlova and Egelman, 1992), the layer-line amplitudes in the Fourier transforms of F-actin images reported by them (Fig. 4, *c* and *f*, of Orlova and Egelman, 1992) showed substantially larger changes in the two conditions compared with our data (data not shown).

Conformational change of F-actin induced by increase in ionic strength

Increase in the ionic strength that stabilized F-actin resulted in a significant decrease in the meridional amplitude of the 27-Å layer-line, which is indicative of more even distribution of the mass projected onto the filament. The redistribution of mass may be associated with alteration of the subunit-subunit contact along the filament axis.

The F-actin model proposed by Holmes and his co-workers (Holmes et al., 1990; Lorenz et al., 1993; Tirion et al., 1995) presented two types of inter-subunit contacts: the diagonal contact, the contact between two subunits that belong to the different long-pitch strands, and the axial contact between two subunits within the same long-pitch strand. According to their model, the axial contact along the long-pitch strand is tighter than the diagonal contact. In other words, the backbone of F-actin consists of two long-

pitch strands, which are bridged together by relatively weak diagonal contacts. The axial contacts are extensive, involving broad interface between subdomains 2 and 4 of a subunit and subdomains 1 and 3 of the axial neighbor. These contacts are crucial for actin polymerization, and the broad contacts consist of a number of polar and/or van der Waals interactions. The DNAse-I-binding loop (residues 41–50) on the top of the subdomain 2 interacts with the C-terminal region in subdomain 1 of the axial neighbor (Khaitlina et al., 1993; Kim and Reisler, 1996; Hegyi et al., 1998). The conformation of the DNAse-I-binding loop is affected by such perturbation as truncation of the C-terminal region or binding of some types of cations to actin, thereby the polymerization properties are modified (Strzelecka-Golaszewska et al., 1995; Moraczewska et al., 1999). Subdomain 2 has been shown to have at least three classes of the conformation based upon its appearance in three-dimensional reconstruction image (Orlova and Egelman, 1995). Increase in the ionic strength by adding KCl inhibits the trypsin cleavage of loop 61–69 within subdomain 2 (Strzelecka-Golaszewska et al., 1996).

In the F-actin model, the loop 61–69 together with the DNase-I-binding loop (41–50) are involved in the axial inter-subunit contacts with subdomain 3 of the adjacent subunit. An extension of either of the two loops, the DNase-I-binding loop more likely, in the axial direction could be responsible for the observed decrease in the meridional amplitude of the 27-Å layer-line, as such conformational change would strengthen the inter-subunit contacts and thereby stabilize the F-actin structure.

Change in twist by lowering solvent pH

Our results showed that the long-pitch 2-start helix becomes less twisted by lowering the solvent pH or by replacing NaCl with LiCl; the helical symmetry was 2.161 subunits per turn of the 1-start helix (12.968/6) at pH 8, whereas it was 2.159 subunits per turn (12.952/6) at pH 6 or in the solvent containing LiCl. A slight change in the diagonal contacts should be responsible for these changes.

According to Holmes' model, the most extensive diagonal contact between the two strands is formed between the hydrophobic plug and the hydrophobic pocket. The hydrophobic plug, located between subdomains 3 and 4 (residues 269–272), which forms a finger-like protrusion extending across the filament axis to the opposite strand, interacts with the hydrophobic pocket formed by residues in the interface between subdomain 2 and subdomain 3 of the axially adjacent two subunits in the opposite strand. This trimeric contact is supposed to be crucial for the nucleus formation in the polymerization process. For the contact, hydrophobic interactions were hypothetically proposed (Holmes et al., 1990, Lorenz et al., 1993), and this proposal was supported by experiments using mutant actin of yeast. Weakening of the hydrophobicity in the hydrophobic plug, by a single

replacement of Leu267 to Asp (Chen et al., 1993) or by double replacements of Val266 to Gly and Leu267 to Gly (Kuang and Rubenstein, 1997), resulted in a cold-sensitive polymerization defect. Furthermore, these amino acid replacements impaired the nucleation and made F-actin less stable after F-actin is formed.

As reported previously, the critical concentration for actin polymerization is decreased and the nucleus for polymerization is stabilized as the solvent pH is lowered from 8 to 6 (Zimmerle and Frieden, 1988b; Wang et al., 1989; Sampath and Pollard, 1991) or by using LiCl as the polymerizing salt (Colombo et al., 1991). These changes of properties might be accounted for by strengthening of the diagonal contact, including the hydrophobic interactions between the plug and the pocket. This perturbation in the diagonal contacts would affect the positions of two long-pitch 2-start helical strands. Another diagonal contact near the filament surface has been proposed between subdomain 4 and subdomain 1 of the diagonal neighbor (Orlova and Egelman, 1992, 1995; Tirion et al., 1995), although this was not shown in the Holmes' model. According to Orlova and Egelman (1992, 1995), this contact has at least three different appearances in electron micrographs: strong, moderate, and absent. Although they did not point out the relation between the appearances and the helical symmetry, modification of this outer diagonal contact would also affect the filament twist.

Origin of conformational changes induced by lowering pH

It is difficult to suppose that lowering pH gives rise to a direct perturbation of the trimeric contact region, including the hydrophobic interactions. Rather, some changes caused in other regions may have some structural influences on the trimeric contact region indirectly. This idea is plausible because there must be close communication between multiple regions of actin, such as the ATP-binding site, the DNAse-I-binding loop, the C-terminal segment, and the hydrophobic plug, and any small, local perturbation could be propagated to remote regions within the molecule (Chen et al., 1993; Kuang and Rubenstein, 1997). However, the sites altered by lowering pH could not be identified in a low-resolution map.

The pH-titration curve of proton binding to actin shows a gentle slope, and the number of negative charges of actin decreases from 30 to 10 as pH decreases from 8 to 6 (Martonosi et al., 1964). It is difficult to identify the residues that are neutralized and affected on the contacts. Nevertheless, there are some interesting reports that give us some suggestions. Actin polymerizes spontaneously at pH below 6.8 (Martonosi et al., 1964), and the fluorescence from G-actin labeled at Cys-374 with IAEDANS, which reports the G-actin conformation, is pH dependent in a manner similar to the titration curve of protonation of a

single class of residues with an approximate pK of 6.8 (Zimmerle and Frieden, 1988a). The structural changes in the hydrophobic contact region may be associated with the protonation of residues with an approximate pK of 6.8 in the actin surface region. Candidates might be either histidine or a carboxyl-carboxylate pair. The latter is known to exhibit an anomalously high pK when the pair is forced to be located in the close proximity by a protein structure or protein-protein interaction (Caspar, 1963).

Another possible explanation for the pH-dependent symmetry change is the binding of Pi to the nucleotide-binding site of actin. The apparent dissociation constant of Pi to the ATP-binding site on actin increases with decrease in pH, because of the increase in the fraction of $H_2PO_4^-$ species (Carlier and Pantaloni, 1988). This leads to an increase in the fraction of actin species bound to ADP and Pi. Because the nucleotide-binding site and the hydrophobic contact region communicate each other (Kuang and Rubenstein, 1997), the binding of Pi to the nucleotide-binding site may change the position and orientation of a subunit relative to the others, resulting in a symmetry change. This idea is consistent with a finding by electron microscopy that F-ADP-BeF$_4$-actin, an analog of the F-ADP-Pi-actin state, showed less twist as compared with F-ADP-actin (Orlova and Egelman, 1992). A preliminary analysis of our fiber diffraction patterns also supports the idea. The difference map between F-actin at pH 6 and pH 8 was constructed using the phases calculated from the F-actin coordinates by Lorenz et al. (1993). In the resulting map (data not shown), a negative peak (less mass at pH 6) was in the center of F-actin near the trimeric contacts, whereas a positive peak (more mass at pH 6) was near the nucleotide-binding site. This is consistent with the idea that lowering pH promotes Pi binding to the nucleotide-binding site, which induces conformational change in the hydrophobic trimeric contact region, although the interpretation is preliminary because the intensity data used are limited to low resolution.

REFERENCES

Belmont, L. D., and D. G. Drubin. 1998. The yeast V159N actin mutant reveals roles for actin dynamics in vivo. *J Cell Biol.* 142:1289–1299.

Bremer, A., R. C. Millonig, R. Sütterlin, A. Engel, T. D. Pollard, and U. Aebi. 1991. The structural basis for the intrinsic disorder of actin filament: the "lateral slipping" model. *J. Cell Biol.* 115:689–703.

Carlier, M. F. 1991. Actin: protein structure and filament dynamics. *J. Biol. Chem.* 266:1–4.

Carlier, M. F., and D. Pantaloni. 1988. Binding of phosphate to F-ADP-actin and role of ADP-Pi-actin in ATP actin polymerization. *J. Biol. Chem.* 263:817–825.

Caspar, D. L. D. 1963. Assembly and stability of the tobacco mosaic virus particle. *Adv. Protein Chem.* 18:37–121.

Chen, X., R. K. Cook, and P. A. Rubenstein. 1993. Yeast actin with a mutation in the "hydrophobic plug" between subdomain 3 and 4 (L2667D) displays a cold-sensitive polymerization defect. *J. Cell Biol.* 123:1185–1195.

Cochran, W., F. H. Crick, and V. Vand. 1952. The structure of synthetic polypeptides. I. The transform of atoms on a helix. *Acta Cryst.* 5:777–781.

Colombo, R., A. Milzani, and I. D. Donne. 1991. Lithium increases actin polymerization rates by enhancing the nucleation step. *J. Mol. Biol.* 217:401–404.

Hanson, J., and S. Lowy. 1963. The structure of F-actin and of actin filaments isolated from muscle. *J. Mol. Biol.* 6:46–60.

Hegyi, G., M. Mak, E. Kim, M. Elzinga, A. Muhlrad, and E. Reisler. 1998. Intrastrand cross-linked actin between Gln-41 and Cys-374. I. Mapping of sites cross-linked in F-actin by *N*-(4-azido-2-nitrophenyl) putrescine. *Biochemistry.* 37:17784–17792.

Holmes, K. C., D. Popp, W. Gebhard, and W. Kabsch. 1990. Atomic model of the actin filament. *Nature.* 347:44–49.

Huxley, H. E., and W. Brown. 1967. The low-angle x-ray diagram of vertebrate striated muscle and its behavior during contraction and rigor. *J. Mol. Biol.* 30:383–434.

Kabsch, W., H. G. Mannherz, D. Suck, E. F. Pai, and K. C. Holmes. 1990. Atomic structure of the actin: DNase I complex. *Nature.* 347:37–44.

Khaitlina, S. and H. Hinssen. 1997. Conformational changes in actin induced by its interaction with gelsolin. *Biophys. J.* 73:929–937.

Khaitlina, S. Y., J. Moraczewska, and H. Strzelecka-Golaszewska. 1993. The actin/actin interactions involving the N-terminus of the DNase-I-binding loop are crucial for stabilization of the actin filament. *Eur. J. Biochem.* 218:911–920.

Kim, E., and E. Reisler. 1996. Intermolecularcoupling between loop 38–52 and the C-terminus in actin filaments. *Biophys. J.* 71:1914–1919.

Klug, A., F. H. Crick, and H. W. Wyckoff. 1958. Diffraction by helical structures. *Acta Cryst.* 11:199–213.

Korn, E. D. 1982. Actin polymerization and its regulation by proteins form nonmuscle cells. *Physiol. Rev.* 62:672–737.

Kouyama, T., and K. Mihashi. 1981. Fluorimetry study of *N*-(1-pyrenyl)iodoacetamide-labelled F-actin. Local structural change of actin protomer both on polymerization and on binding of heavy meromyosin. *Eur. J. Biochem.* 114:33–38.

Kuang, B., and P. A. Rubenstein. 1997. Beryllium fluoride and phalloidin restore polymerizability of a mutant yeast actin (V266G, L267G) with severely decreased hydrophobicity in a subdomain 3/4 loop. *J. Biol. Chem.* 272:1237–1247.

Kurokawa, H., W. Fujii, K. Ohmi, T. Sakurai, and Y. Nonomura. 1990. Simple and rapid purification of brevin. *Biochem. Biophys. Res. Commun.* 168:451–457.

Lepault, J., J. L. Ranck, I. Erk, and M. F. Calier. 1994. Small angle x-ray scattering and electron cryomicroscopy study of actin filaments: role of the bound nucleotide in the structure of F-actin. *J. Struct. Biol.* 112:79–91.

Lorenz, M., D. Popp, and K. C. Holmes. 1993. Refinement of the F-actin model against x-ray fiber diffraction data by the use of a directed mutation algorithm. *J. Mol. Biol.* 234:826–836.

Martonosi, A., C. M. Molino, and J. Gergely. 1964. The binding of divalent cations to actin. *J. Biol. Chem.* 239:1057–1064.

McGough, A., B. Pope, W. Chiu, and A. Weeds. 1997. Cofilin changes the twist of F-actin: implications for actin filament dynamics and cellular function. *J. Cell Biol.* 138:771–781.

Moraczewska, J., B. Wawro, K. Seguro., and H. Strzelecka-Golaszewska. 1999. Divalent cation-, nucleotide-, and polymerization-dependent changes in the conformation of subdomain 2 of actin. *Biophys. J.* 77:373–385.

Oda, T., K. Makino, I. Yamashita, K. Namba, and Y. Maéda. 1998. Effect of the length and effective diameter of F-actin on the filament orientation in liquid crystalline sols measured by x-ray fiber diffraction. *Biophys. J.* 75:2672–2681.

Oda, T., K. Makino I. Yamashita, K. Namba, and Y. Maéda. 2000. The helical parameters of F-actin precisely determined from x-ray fiber diffraction of well-oriented sols. *In* Molecular Interactions of Actin: Actin Structure and Actin-Binding Proteins. C. G. dos Remedios and D. D. Thomas, editors. Springer Verlag, Heidelberg. 43–58.

Oosawa, F., and M. Kasai. 1962. A theory of linear and helical aggregations of macromolecules. *J. Mol. Biol.* 4:10–21.

Oosawa, F., and M. Kasai. 1971. Actin. *In* Subunits in Biological Systems. S. N.Timasheff and G. D. Fasman, editors. Dekker, New York. 261–322.

Orlova, A., and E. H. Egelman. 1992. Structural basis for the destabilization of F-actin by phosphate release following ATP hydrolysis. *J. Mol. Biol.* 227:1043–1053.

Orlova, A., and E. H. Egelman. 1993. A conformational change in the actin subunit can change the flexibility of the actin filament. *J. Mol. Biol.* 232:334–341.

Orlova, A., and E. H. Egelman. 1995. Structural dynamics of F-actin. I. Changes in the C terminus. *J. Mol. Biol.* 24:582–597.

Orlova, A., E. Prochniewicz, and E. H. Egelman. 1995. Structural dynamics of F-actin. II. Cooperativity in structural transitions. *J. Mol. Biol.* 245:598–607.

Pan, X. X., and B. R. Ware. 1988. Actin assembly by lithium ions. *Biophys. J.* 53:11–16.

Press, W. H., S. A. Teukolsky, W. T. Vetterling, and B. P. Flannery. 1994. Numerical Recipes in C.The Art of Scientific Computing. Cambridge University Press, Cambridge.

Prochniewicz, E., Q. Zhang, P. A. Janmey, and D. D. Thomas. 1996. Cooperativity in F-actin: binding of gelsolin at the barbed end affects structure and dynamics of the whole filament. *J. Mol. Biol.* 260: 756–766.

Sampath, P., and T. D. Pollard. 1991. Effect of cytochalasin, phalloidin, and pH on the elongation of actin filaments. *Biochemistry.* 30: 1973–1980.

Spudich, J. A., and S. Watt. 1971. The regulation of rabbit skeletal muscle contraction. I. Biochemical studies of the interaction of the tropomyosin-troponin complex with actin and the proteolytic fragments of myosin. *J. Biol. Chem.* 246:4866–4871.

Strzelecka-Golaszewska, H., M. Mossakowska, A. Wozniak, I. Moraczewska. and H. Nakayama. 1995. Long-range conformational effects of proteolytic removal of the last three residues of actin. *Biochem. J.* 307:527–534.

Strzelecka-Golaszewska, H., A. Wozniak, T. Hult, and U. Lindberg. 1996. Effects of the type of divalent cation, Ca^{2+} or Mg^{2+}, bound at the high-affinity site and of the ionic composition of the solution on the structure of F-actin. *Biochem. J.* 316:713–721.

Suzuki, A., and T. Ito. 1996. Polymorphism of F-actin assembly. II. Effects of barbed end capping on F-actin assembly. *Biochemistry.* 35: 5245–5249.

Tirion, M., D. ben-Avraham, M. Lorenz, and K. C. Holmes. 1995. Normal modes as refinement parameters for the F-actin model. *Biophys. J.* 68:5–12.

Wang, F., R. V. Sampogna, and B. R. Ware. 1989. pH dependence of actin self-assembly. *Biophys. J.* 55:293–298.

Yamashita, I., K. Hasegawa, H. Suzuki, F. Vondervist., Y. Mimori-Kiyosue, and K. Namba. 1998. Structure and switching of bacterial flagellar filament studied by x-ray fiber diffraction. *Nat. Struct. Biol.* 5:125–132.

Yamashita, I., F. Vonderviszt, Y. Mimori, H. Suzuki, K. Oosawa, and K. Namba. 1995. Radial mass analysis of the flagellar filament of *Salmonella*: implications for the subunit folding. *J. Mol. Biol.* 253: 547–558.

Zimmerle, C. T., and C. Frieden. 1988a. pH-induced changes in G-actin conformation and metal affinity. *Biochemistry.* 27:7759–7765.

Zimmerle, C. T., and C. Frieden. 1988b. Effect of pH on the mechanism of actin polymerization. *Biochemistry.* 27:7766–7772.